nature communications

Article

https://doi.org/10.1038/s41467-025-62634-9

Ligand supplementation restores the cancer therapy efficacy of the antirheumatic drug auranofin from serum inactivation

Received: 18 October 2024

Accepted: 28 July 2025

Published online: 09 August 2025

Check for updates

Yuan Wang[1,4], Bei Cao[2,3,4], Qianqian Wang[1,4], Sinan Zhong[1], Xin Fang[1], Junjian Wang[1] ✉, Albert S. C. Chan[1], Xiaolin Xiong[1] ✉ & Taotao Zou[1] ✉

Auranofin, an FDA-approved antirheumatic gold drug, has gained ongoing interest in clinical studies for treating advanced or recurrent tumors. However, gold ion's dynamic thiol exchange nature strongly attenuates its bioactivity due to the fast formation of covalent albumin-gold adducts. Here we report that newly-added thiols can modulate the dynamic albumin-gold binding and recover the therapeutic efficacy. Initially, we find that auranofin supplemented with its own thiol ligand, TGTA (1-thio-β-D-glucose tetraacetate), significantly restores the anticancer activities in cells and patient-derived xenograft models. Then, screening a collection of ligand fragments followed by machine learning evaluation unveils diverse synergizing thiols, including pantethine, that effectuate auranofin at a low dosage for rheumatoid arthritis. Interestingly, the thiol exchange inside cells accounts for a cuproptosis-like phenotype that auranofin induces. Together, we believe the ligand-enabled dynamic modulation strategy is of value to researchers and clinicians contemplating metallodrugs and ligand-like molecules in cancer therapy.

As representative anticancer agents, platinum drugs were taken by 10–20% of all cancer patients (https://www.cancer.gov/research/progress/discovery/cisplatin). Their therapeutic value continues to be high in the clinic and clinical trials as synergistic agents with other cutting-edge cancer therapies[1–6]. The potent bioactivities underlying platinum drugs are associated with their distinctive ligand exchange kinetics before and after entering cancer cells. In blood, cisplatin, for example, displays fair stability against hydrolysis and off-target binding due to the concentrated chloride, but once inside cancer cells, it undergoes dynamic ligand hydrolysis and exchange to end up with binding biomolecular targets[7–9]. Unfortunately, such a kinetic trait seems hardly endowed by other metal compounds[10], and no metal anticancer drugs other than platinum have been approved so far[11–14]. Extensive efforts have been made on the stability-reactivity trade-off of metallodrugs based on structure-activity-relationship in the past decades[1,11,13–21] but with limited clinic success.

In addition to designing new molecules, repurposing previously approved metallodrugs appears to be a more efficient and less costly way[22–26]. In this regard, auranofin, a US Food and Drug Administration (FDA)-approved gold drug for rheumatoid arthritis (RA), has undergone substantial preclinical and clinical studies for repurposing against advanced or recurrent cancers[27–34]. This rheumatic gold drug has a high binding affinity to cysteine- and selenocysteine-containing proteins and acts as a pro-oxidative agent to kill various types of cancer cells, including the cisplatin-resistant variants[34–48]. Still, a similar challenge is that the dynamic thiol exchange (DyThex) nature of gold leads to instability once the drug encounters the off-target thiols before reaching the tumor. In particular, the most abundant serum protein

[1]State Key Laboratory of Anti-Infective Drug Discovery and Development, Guangdong Provincial Key Laboratory of Chiral Molecule and Drug Discovery, School of Pharmaceutical Sciences, Sun Yat-Sen University, Guangzhou, China. [2]College of Education Sciences, The Hong Kong University of Science and Technology (Guangzhou), Guangzhou, China. [3]Warshel Institute for Computational Biology, and General Education Division, The Chinese University of Hong Kong, Shenzhen, China. [4]These authors contributed equally: Yuan Wang, Bei Cao, Qianqian Wang. ✉e-mail: wangjj87@mail.sysu.edu.cn; xiongxlin@mail.sysu.edu.cn; zoutt3@mail.sysu.edu.cn

albumin (~40 mg/mL) with a free thiol group (Cys34) can displace the TGTA (1-thio-β-D-glucose tetraacetate) ligand of auranofin to form a protein-gold adduct in a fast and complete manner[49–51], which leads to poor bioavailability and unsatisfactory anticancer efficacy in vivo[52–54].

Given that the albumin-auranofin binding is a "thiol-to-thiol" exchange reaction, we conceived the possibility of rescuing active gold by additionally introducing small thiol molecules to modulate the dynamic equilibrium. Herein, we report that supplementing auranofin with TGTA enhanced the anticancer efficacy in both cell lines and animal models, including patient-derived tumor xenografts. Further, cell-based screening of >200 commercially available ligand fragments followed by a machine learning evaluation helped identify a group of thiol molecules, particularly pantethine, that can boost the anticancer activity of auranofin at a low dosage equal to those permitted for treating RA in humans. Interestingly, we also found that the intracellular DyThex enables auranofin to engage in a cuproptosis-like mode of action.

Results

Thiol exchange with auranofin in the multidrug combo CUSP9v3

Some clinical trials in recent years have been associated with auranofin (Fig. 1a) for cancer therapy (https://classic.clinicaltrials.gov). Among the trials, NCT02770378 drew our attention as it used 9 drugs (including auranofin) in combination with temozolomide for recurrent glioblastoma treatment[55,56] (Fig. 1b). Each drug was selected for targeting a certain pathway with a synergistic effect against the resistance mechanisms of this cancer. The phase Ib/IIa trial has confirmed the

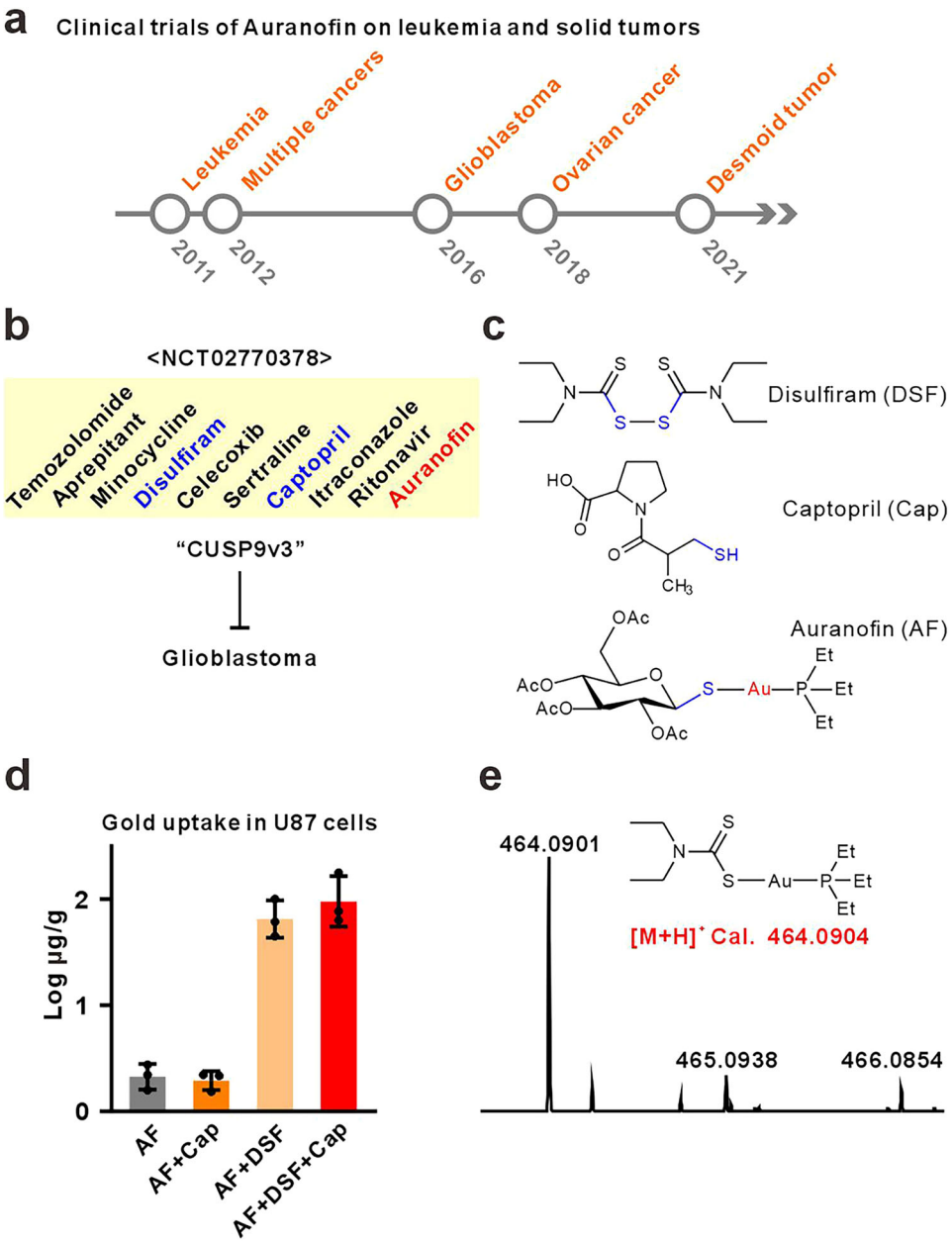

Fig. 1 | Thiol exchange in auranofin-related clinical trials. a a timeline summary of auranofin-repurposing clinical trials on cancer therapy in recent years. **b** drugs used in clinical trial NCT02770378 for glioblastoma. **c** the chemical structures of the indicated drugs. **d** cellular gold uptake affected by the co-treatment with thiol-containing drugs in U87 cells. 3 μM of auranofin was used in all groups with or without DSF (570 μM) or Cap (156 μM) for 10 min at 37 °C. Data are shown as mean ± s. d. of three independent experiments. **e** mass spectrometry identified the formation of a DEDT-gold-phosphine molecule after an in vitro incubation of auranofin (2 μM), captopril (4 μM), and disulfiram (2 μM) for 30 min at 37 °C in methanol. The spectrum was extracted from 463.0000 to 467.0000 *m/z* $[M+H]^+$ values with the predicted *m/z* labeled in red. The result is representative of three independent experiments. Source data are provided as a Source Data file.

safety of the CUSP9v3 treatment regimen, and a randomized phase II trial has also been completed.

Besides auranofin, two thiol-containing drugs, disulfiram and captopril (Fig. 1c), which are in large molar excess (190- and 52-fold as compared to auranofin, respectively), were also included in CUSP9v3. Since the cellular uptake of auranofin is relatively quick (Supplementary Fig. 1a), we sought to check their impacts on auranofin uptake after a short period of coincubation to minimize any possible interference from the thiol drugs on the cell status. The treatments were conducted in the presence of 30% FBS (Fetal Bovine Serum) to mimic the physiological interference from albumins, using the co-treatments on a glioblastoma cell line U87 following their ratios in CUSP9v3. Interestingly, the addition of disulfiram largely enhanced the cellular uptake of gold by over 50-fold at this serum-containing condition (Fig. 1d). Captopril, however, had no direct effect on the uptake (Fig. 1d). Also, data showed that the enhanced gold uptake in 30% FBS by adding disulfiram was equal to 32.6% of the uptake in serum-free conditions (Supplementary Fig. 1b). Moreover, increasing the concentrations of either thiol drug will lead to an enhanced cytotoxicity (Supplementary Fig. 1c,d). Incubating the three drugs in aqueous solution generated a compound in which diethyldithiocarbamate (DEDT), the reduced product of disulfiram, displaced the TGTA ligand in auranofin (Fig. 1e). Thus, the drug interactions occur in this multidrug combo that may contribute to the bioavailability of gold.

Albumin blockade on auranofin is reversed by excess TGTA ligand

In CUSP9v3, the reduced DEDT is at a large excess, so we considered that it may compete with albumin, impeding the formation of cell-impermeable protein-gold complex and improving the bioavailability of gold. However, DEDT has been known to inhibit NPL4 and cause strong cytotoxicity[57]. Therefore, we sought to harness TGTA, a ligand with minimal cytotoxicity ($IC_{50} > 300\ \mu M$), to further support our hypothesis that excess TGTA ligand may shift the equilibrium from the albumin-gold adduct back to auranofin and recover cytotoxicity (Fig. 2a). First, we found that the blocking effects were positively correlated to fetal bovine serum (FBS) or human serum albumin (HSA) concentrations in the media (Supplementary Fig. 2). Next, we monitored the reaction between bovine serum albumin (BSA) and auranofin by High Performance Liquid Chromatography (HPLC). As expected, the peak of auranofin (retention time 3.78 min) disappeared when mixed with albumin (Fig. 2b), in association with the formation of an albumin-Au-PEt_3 adduct (characterized by High-Resolution Mass Spectrometry, HRMS, Supplementary Fig. 3). Of note, the peak of auranofin reappeared in the LC chromatogram after adding excess TGTA into the albumin-auranofin mixture (Fig. 2b and Supplementary Fig. 4a). The TGTA itself would not affect the auranofin as indicated by the HPLC (Supplementary Fig. 4b). Encouraged by this phenomenon, we tested the effects of TGTA at the cellular level. Interestingly, the gold uptake was significantly reduced with increasing serum concentrations but recovered by supplementing with TGTA (Fig. 2c and Supplementary Fig. 4c). Next, we investigated the effects of adding TGTA on cytotoxicity. While the cytotoxicity of auranofin was largely suppressed by albumins in the serum (Supplementary Fig. 2), a TGTA dose-dependent recovery was found with a fixed concentration of auranofin (Fig. 2d). As a control, the glucose pentaacetate, a thiol-free homolog of TGTA, did not influence cytotoxicity (Fig. 2d). Consistent with increased cellular gold contents and cytotoxicity, the activity of thioredoxin reductase (TrxR), a primary target of auranofin[58–61], was significantly inhibited by the additional TGTA ligands in the living HCT116 cells (Fig. 2e and Supplementary Fig. 4d).

In our experimental setup, the potentiation was observed after a 24-hour co-treatment of auranofin and TGTA. Treating HCT116 cells with 50 μM TGTA alone for 24 hours can induce a certain degree of cellular changes, revealed by transcriptomic and proteomic profiling data (Supplementary Data 1). To check whether these TGTA-induced changes contributed to the enhanced activity of auranofin, we administered auranofin to TGTA-pretreated HCT116 cells. The 24-hour pretreatment was conducted in the same way as the abovementioned omics studies (Supplementary Fig. 5a). Then, the TGTA was washed before adding auranofin. The cellular gold uptake was measured 2 hours after auranofin administration. As the data showed, only the combined treatment, but not the pretreated one, elevated the cellular gold content (Supplementary Fig. 5b). This indicated that a direct interaction is required, supporting the idea of ligand exchanges. We also monitored the cytotoxicity after 24 hours of treatment with auranofin. Consistently, no enhancement of cytotoxicity was seen in the TGTA pretreated cell lines (A549, HCT116, and PC9), while the co-treatment group resulted in enhanced cytotoxicity (Supplementary Fig. 5c). These all suggested that the auranofin potentiation is mainly through ligand exchanges rather than the TGTA-driven cellular changes.

Admittedly, there is still a relatively moderate potentiation (about 2.5-fold) of auranofin's cell uptake by TGTA in serum-free conditions, compared to almost 6.0-fold potentiation in 10% FBS (Supplementary Fig. 4c). In PC9 cells pretreated with auranofin in serum-free media, knocking down the multidrug resistance protein 1 (MRP1) resulted in an increased sensitivity to auranofin (Supplementary Fig. 6a). This efflux pump seems to account for auranofin resistance under serum-free conditions. Thus, although rescuing the albumin-bound gold by TGTA mainly potentiates auranofin in the presence of serum, TGTA may also function on other cellular mechanisms to help increase gold content in cells under some special situations (Supplementary Fig. 6b).

Next, we examined the efficacy of the "auranofin + TGTA" combo in mouse models (Fig. 2f). An early study has claimed that only P388 leukemia, out of 15 tumor mouse models (blood and solid tumors), was sensitive to auranofin treatment at a dose of 12 mg/kg intraperitoneally[53]. Later works showed that 10 mg/kg of auranofin was typically required to achieve the anticancer effect in murine models[62–64]. Here, we used 3 mg/kg, a dosage with minimal anti-tumor activity in vivo in auranofin treatment alone. For TGTA toxicity, 100 mg/kg of this compound was injected intraperitoneally for three consecutive days. We did not observe weight loss or other side effects in the mice (Supplementary Fig. 7a). In the mice-bearing HCT116 xenograft, TGTA (40 mg/kg) significantly enhanced the tumor suppression of auranofin compared to vehicle control after intraperitoneal injection. Still, TGTA or auranofin alone failed to suppress tumor growth. In addition, we found an elevated level of tumoral gold content when treating the tumor-bearing mice with the combo group (Supplementary Fig. 7b). Then, we sought to evaluate the responses in two patient-derived xenograft (PDX) models, non-small cell lung carcinoma (NSCLC) and triple-negative breast cancer (TNBC), respectively. Similar results were observed in these two PDX models (Fig. 2f). To further check the impact of our combo on mouse physiology, we monitored the body weight of each mouse. In all three models, we found no mouse death or noticeable change in mouse body weight (Supplementary Fig. 8a). Besides, no pathological features were observed by inspecting internal organs (heart, kidney, liver, lung, spleen) in the mice of NSCLC PDX models (Supplementary Fig. 8b). These results suggested that TGTA can potentiate the antitumor activity of auranofin without apparent toxicity.

Ligand screening unveils molecules able to synergize with auranofin

The successful use of TGTA drove us to mine more ligands with synergistic activities. A collection of 252 commercially available ligand fragments containing N, O, S, or P binding sites was screened at a constant concentration (50 μM) for their synergistic effect on auranofin. The cell viability of the combo group versus auranofin alone

https://doi.org/10.1038/s41467-025-62634-9

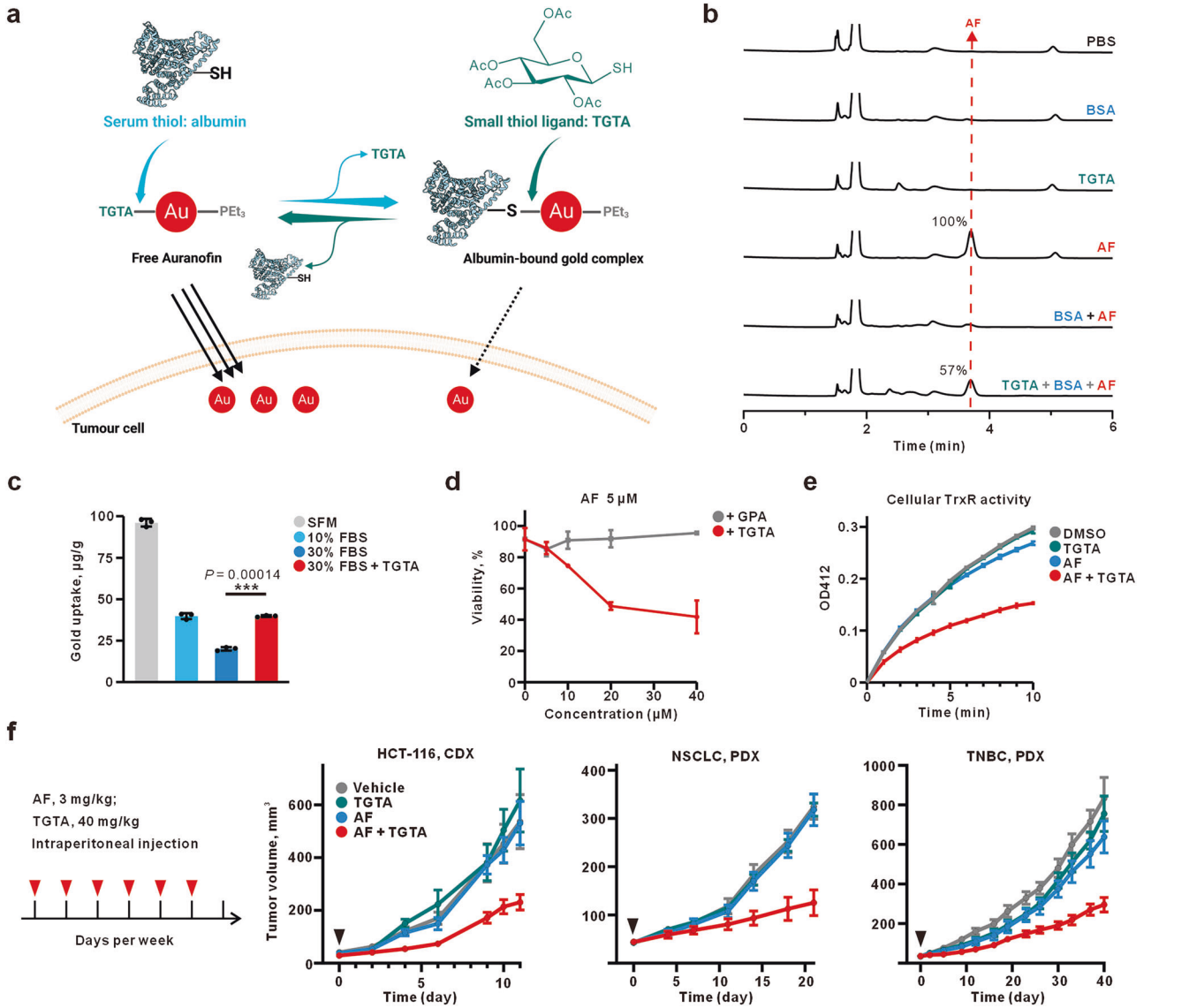

Fig. 2 | TGTA restores the anticancer activity of albumin-bound auranofin. a a scheme for harnessing the dynamic thiol exchange to restore anticancer efficacy from albumin-bound gold. TGTA, thioglucose tetraacetate. Created in BioRender. Xiong, X. (2025) https://BioRender.com/zpgjm50. **b** HPLC analysis at 214 nm on the thiol exchange reaction in vitro. 1 mM of auranofin was added to 1.0 mL of 4 mM solution of BSA and then reacted at 37 °C for 60 min in a shaker. 5 mM of TGTA (5 equivalents) was used. The peak of auranofin was marked by a dotted red line. **c** cellular gold uptake of HCT116 cells under indicated conditions of FBS for 1 h. 3 μM of auranofin was used in all groups with or without TGTA (50 μM). The values were normalized by the protein amount extracted. Data are shown as mean ± s. d. of three independent experiments. Significance was calculated by an unpaired, two-tailed *t*-test. Significance was defined as $p < 0.05$. **d** dose-dependent cytotoxicity boosting of auranofin by glucose homologs after 24-hour treatments. GPA, Glucose pentaacetate. **e**, measuring cellular thioredoxin reductase (TrxR) activity using HCT116 upon indicated treatments. HCT116 cells in RPMI + 30% FBS were incubated with 0.5 μM auranofin and/or 50 μM TGTA for 1 h before cell lysis for TrxR activity detection. For **d**, **e**, mean ± s. d., 3 biological replicates. **f** mouse models to evaluate the in vivo tumor suppression of auranofin. Drugs were injected intraperitoneally 6 times per week, and the initial administration day was marked by black arrows. An HCT116 xenograft and two patient-derived xenografts (non-small cell lung carcinoma and triple-negative breast cancer) were conducted. HCT116 tumors: Vehicle, $n = 7$ mice; TGTA, $n = 6$ mice; AF, $n = 6$ mice; AF + TGTA, $n = 9$ mice. NSCLC PDX tumors: Vehicle, $n = 7$ mice; TGTA, $n = 6$ mice; AF, $n = 6$ mice; AF + TGTA, $n = 7$ mice. TNBC PDX tumors: Vehicle, $n = 9$ mice; TGTA, $n = 9$ mice; AF, $n = 8$ mice; AF + TGTA, $n = 8$ mice. Data were shown as mean ± s. e. m. Source data are provided as a Source Data file.

("A + L"/A) was plotted as the effectiveness ratio (Fig. 3a). We selected those with a ratio less than 0.3 as the primary pool of active candidates and then tested their own cytotoxicity (Fig. 3b). Finally, 14 compounds with synergistic effects but also negligible cytotoxicity (<10 %) were picked as the "effective" ones. Notably, thiol- (including disulfide-) or phosphine-containing ones were significantly enriched in the effective pool (Fig. 3c), in line with the high affinity of gold ions toward these two types of ligands. Computational calculation using density functional theory (DFT) on different types of ligands (Cl, N, O, P, S) supports the screening outcomes as only thiol and phosphine ligands can lead to favorable shift of ligand exchange equilibrium (chemical equilibrium constant *K* close to 1 or higher, Supplementary Fig. 9). As a more physiologically relevant type of molecules, the effective thiols or disulfides are promising ligand to potentiate auranofin with only moderate cytotoxicity exhibited by themselves (Supplementary Fig. 10), we then focused on the chemical features dictating their effectiveness. Based on the 354 calculated chemical descriptors for each thiol-containing molecule, we trained a random forest classification model to weigh their importance toward the effectiveness (Fig. 3d). As the results showed, most descriptors related to molecular

https://doi.org/10.1038/s41467-025-62634-9

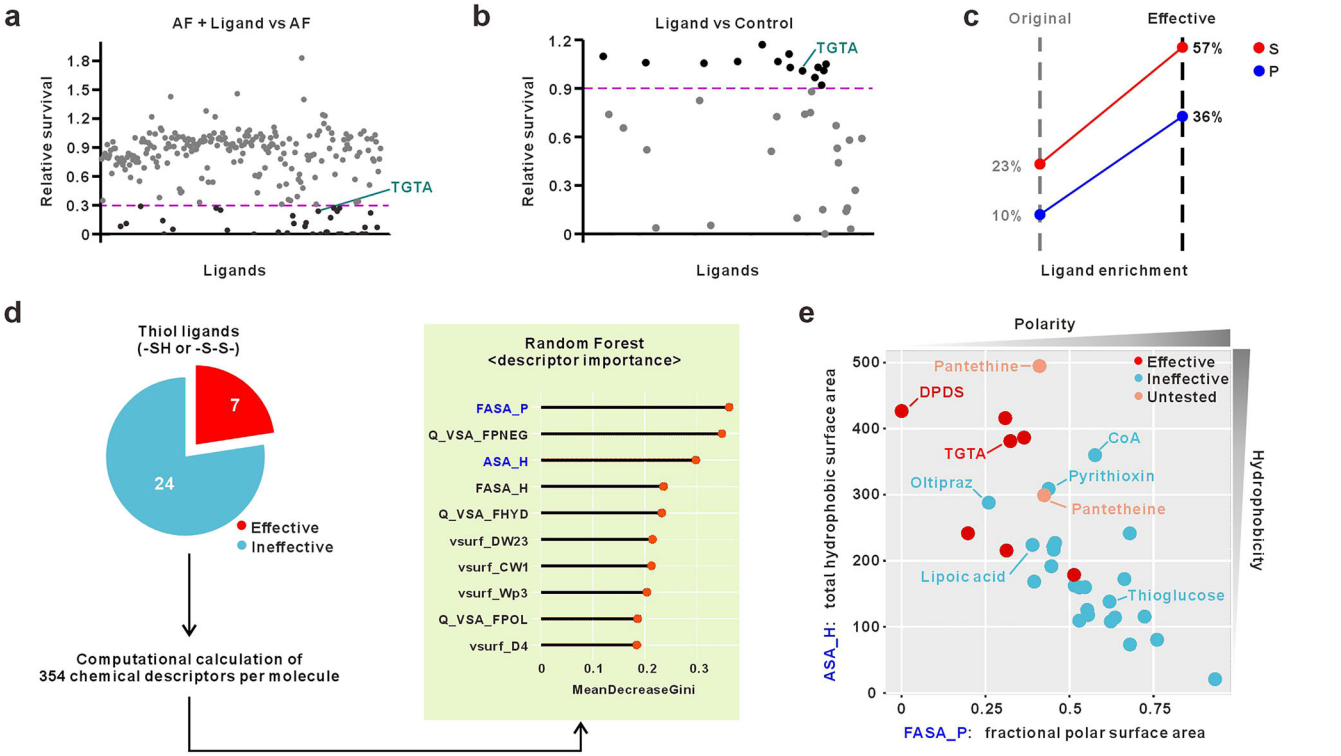

Fig. 3 | Ligand screening in synergy with auranofin. a PC9 cell viability in response to co-treatments using 5 μM auranofin with 50 μM ligands from a chemical library containing 252 small molecules. Ligands with values under 0.3 (dotted line in pink) were picked for the next experiments. **b** a counter-screening on the self-toxicity of the picked ligands. Ligands with less than 10% toxicity were picked as the effective synergistic ones. **c** percentages of sulfur- (S) or phospho- (P) containing molecules in the original and effective ligands were compared. **d** a workflow evaluating the synergy-associated chemical features using random forest classification based on 354 descriptors calculated by MOE software. The top 10 descriptors ranked by importance were listed with their MeanDecreaseGini values. **e** plotting the thiol ligands by their values of two descriptors, FASA_P and ASA_H. Effective, ineffective, and untested molecules were colored as indicated. Names of some ligands were shown. Source data are provided as a Source Data file.

polarity and hydrophobicity were ranked top of all (Fig. 3d). This indicated that ligands with suitable lipophilicity can shuttle gold ions into the cells.

To visualize the classification, we plotted the thiol ligands using two top-ranking descriptors, FASA_P (fractional polar surface area) for polarity and ASA_H (total hydrophobic surface area) for hydrophobicity (Fig. 3e). According to the plot, effective ones were preferably located in the high hydrophobicity and low polarity region. Diphenyl disulfide (DPDS), with the most hydrophobicity indicated by the plot, is a chemical reagent frequently used in organic synthesis. Noteworthily, a recent report claimed an anti-breast cancer activity of this compound in an apoptosis-promoting mechanism[65]. Oltipraz and pyrithioxin are ineffective ligands but are located near the region of the effective ligand in the plot. Reasonably, these two agents still showed a potential to synergize auranofin in the primary screening with effectiveness ratios of 0.57 and 0.31, respectively (close to the set threshold of 0.3). Based on the analysis above, we hypothesized that chemical parameters related to hydrophobicity can serve as important criteria for choosing effective thiol ligands. In addition, we checked the contribution of the newly formed molecules to enhanced cytotoxicity by using two of the effective ligands, sodium thiophenolate and 4-chlorothiophenol. Both can react with the auranofin directly to replace the TGTA from the gold center to result in gold species. As the results showed (Supplementary Fig. 11), only the new gold complexes formed by thiophenolate, but not 4-chlorothiophenol, conferred a higher gold uptake and cytotoxicity on HCT116 cells in serum-free conditions. These indicated that ligands' chemical features may determine the bioactivity of the newly formed gold molecules after thiol exchanges in a case-by-case situation.

Next, we wondered whether hydrophilic thiols can shuttle gold ions to certain cell types. To this end, a further screening using hydrophilic but physiologically relevant thiols in a higher concentration on ten cell lines was performed (Fig. 4a). This comprises coenzyme A (CoA)[66], some of its derivatives, and two other thiols (lipoic acid, thioglucose). However, CoA, lipoic acid, and thioglucose were still less effective, although a relatively high auranofin-boosting activity was seen by CoA in Jurkat T cells. Interestingly, pantethine and its reduced monomeric form pantetheine came up with the strongest synergistic effects.

Pantethine potently synergizes with auranofin both in vitro and in vivo

Pantethine, composed of pantothenate and cysteamine moieties (also the molecular fragments of CoA), is a dietary supplement for pantothenate-fueled CoA biosynthesis. Noteworthily, it can be orally administered at doses up to 1.2 g per day[67], of which the good safety renders it a promising candidate as a clinical adjuvant for auranofin. Like TGTA, we found a dose-dependent auranofin-boosting manner of pantethine (Fig. 4b) along with an increase of cellular gold (Fig. 4c). To further verify the involvement of the ligand exchange mechanism, we compared several structure-related molecules, such as pantethine, pantetheine, cysteamine, and pantothenate, for their abilities in synergizing auranofin. All these small molecules are related to the pantothenate metabolism[68]. For the lack of thiol group, pantothenate failed to boost auranofin (Fig. 4d). Pantetheine and its metabolic product cysteamine conferred a similar synergistic effect, and combo using cysteamine with pantothenate did not further enhance the effect (Fig. 4d). These results ruled out the engagement of pantothenate

https://doi.org/10.1038/s41467-025-62634-9

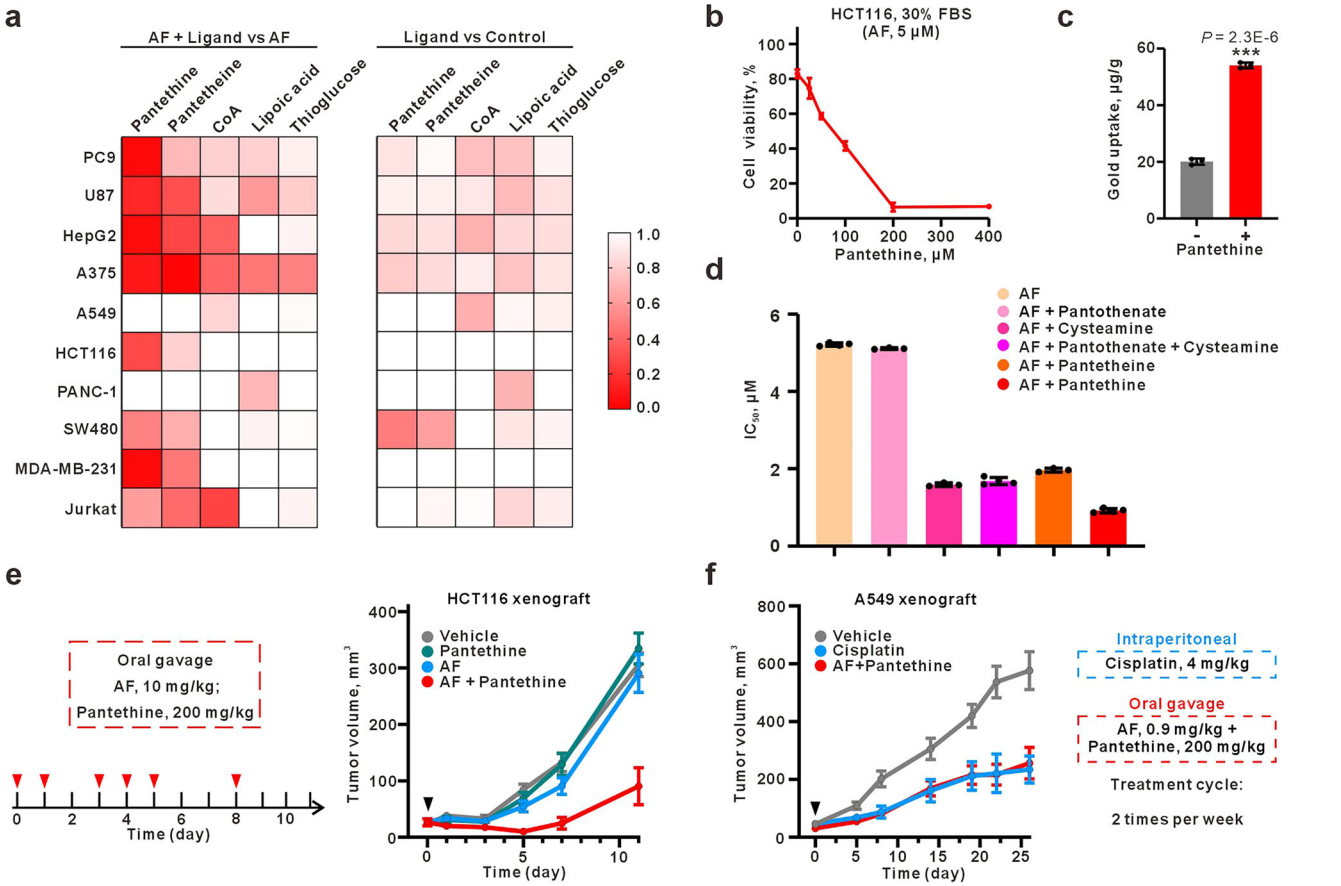

Fig. 4 | Synergistic effect of pantethine on auranofin. a a small-scale cell line profiling using indicated agents. The color bar represents the mean value of relative survival (24 h) in three independent experiments. 5 μM auranofin was used. Except for pantethine (200 μM), other thiol ligands were all used at 400 μM. All the cells were cultured in HPLM + 30% FBS. **b** the dose-dependent synergy of pantethine with auranofin. The viability after a 24-hour treatment was measured. Data are shown as mean ± s. d. of three independent experiments. Significance was calculated by unpaired, two-tailed *t*-test. **c** cellular gold uptake of HCT116 cells under 3 μM auranofin with or without 200 μM pantethine for 1 h. The values were normalized by the amount of protein extracted. Data are shown as mean ± s. d. of three independent experiments. Significance was calculated by unpaired, two-tailed *t*-test. Significance was defined as $p < 0.05$. **d** the comparison of the synergistic activities with auranofin endowed by different pantothenate derivatives using HCT116 cells in a 24-hour treatment. Except for pantethine (200 μM), its derivatives were all used at 400 μM. Data are shown as mean ± s. d. of 3 biologically independent experiments. Significance was calculated by unpaired, two-tailed *t*-test. **e** mouse models using oral gavage on an HCT116 xenograft. Drugs were administered on the indicated days. **f** an A549 xenograft model to compare the tumor suppression of auranofin-pantethine combo and cisplatin monotherapy. Drug administration was conducted two times per week with indicated concentrations. For **e**, **f**, data were shown as mean ± s. e. m.. HCT116 tumors: Vehicle, $n = 8$ mice; pantethine, $n = 7$ mice; AF, $n = 6$ mice; AF + pantethine, $n = 8$ mice. A549 tumors: Vehicle, $n = 6$ mice; cisplatin, $n = 6$ mice; AF + pantethine, $n = 4$ mice. Source data are provided as a Source Data file.

metabolism in the synergistic effects, reinforcing a thiol-to-thiol exchange mechanism. To further confirm that the thiol exchange mediated by pantethine could happen in a host-mimic condition, we examined the gold speciation under the co-treatment using auranofin and pantethine in human serum. As expected, compound Et_3P-Au-RPT was detected in which pantetheine displaced the TGTA ligand in auranofin (Supplementary Fig. 12a, b). We also measured the ability of pantetheine or pantethine to rescue the protein-bound gold (Supplementary Fig. 12c), with the results showing that both these ligands can reduce the albumin-bound gold content to a similar extent as TGTA.

Encouraged by the results above, we next studied the effects of the "auranofin + pantethine" combo in animal xenografts. Given that pantethine can be taken orally like auranofin, oral gavage was conducted in an HCT116 xenograft. As the results showed (Fig. 4e), while single treatment by auranofin or pantethine did not show any tumor growth inhibition, the combo group led to significant inhibition, similar to the activity of TGTA with intraperitoneal injection. Likewise, the combo of auranofin-pantethine did not affect the body weight and organs of the treated mice (Supplementary Fig. 13a, b). Moreover, this orally available combo allowed the use of auranofin at 0.9 mg/kg, equivalent to the dosage permitted for treating RA in humans[69,70], to significantly suppress tumor growth in an A549 xenograft. The activities of this combo are comparable to an intraperitoneal treatment of cisplatin at 4 mg/kg (Fig. 4f). No loss of body weight was found in this model as well (Supplementary Fig. 13a).

The gold ions can be maintained for a relatively long period in the blood (plasma half-lives of auranofin gold of 1.8 days in rats, 19.5 days in dogs, and 17 days in humans)[37,71,72]. To better understand the influence of pantethine (200 mg/kg) on auranofin (10 mg/kg) in circulation, we monitored the plasma gold levels using Sprague-Dawley rats. In both administration setups as indicated, the gold levels in blood decreased one hour after pantethine administration (Supplementary Fig. 14), indicating a direct alteration in albumin binding.

DyThex drives auranofin to induce a cuproptosis-like cell death type

Besides the pharmacokinetics, next, we sought to investigate whether the DyThex nature of gold contributes to its intracellular mode of action. In the second-round ligand screening, lipoic acid (LA), the organosulfur derivative of octanoic acid, was found to be less effective

https://doi.org/10.1038/s41467-025-62634-9

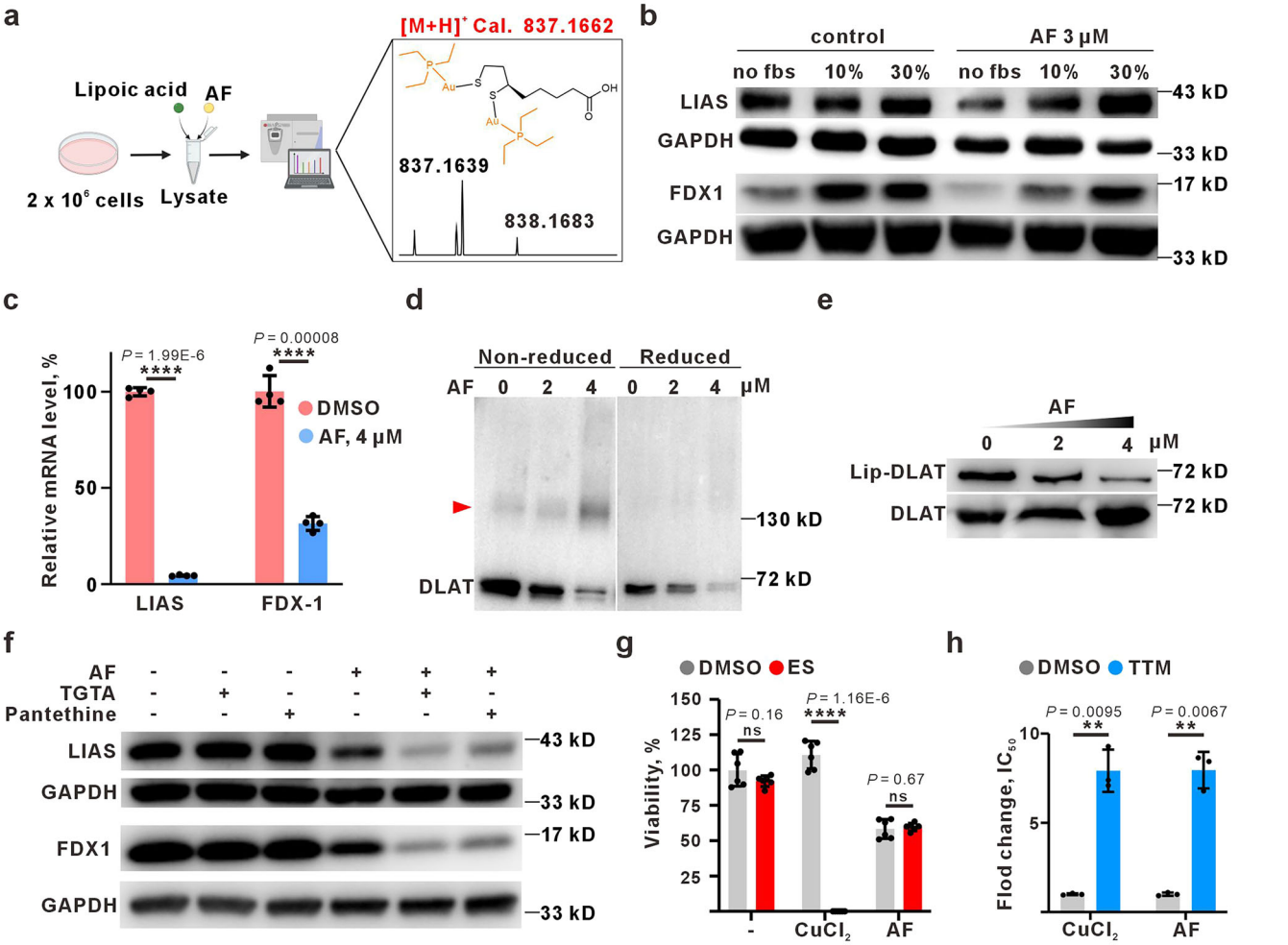

Fig. 5 | Auranofin induces cuproptosis-like cell death by thiol exchange. a mass spectrometry identification of the products after thiol exchange during the 0.5-hour incubation of auranofin (100 μM) and lipoic acid (1 mM) in the cell lysate (500 million cells to 400 μL lysates in ddH_2O). Created in BioRender. Xiong, X. (2025) https://BioRender.com/i289oxu. **b** analysis of the cuproptosis markers (LIAS and FDX1) in HCT116 cells after a 24-hour auranofin treatment in the presence of different concentrations of FBS. The samples derive from the same experiment but different gels for anti-LIAS and anti-FDX1 antibodies were processed in parallel. **c** qRT-PCR analysis of the mRNA levels of indicated genes after a 12-hour treatment with 4 μM auranofin. Data are shown as mean ± s. d. of four independent experiments. Significance was calculated by unpaired, two-tailed *t*-test. Significance was defined as $p < 0.05$. **d** DLAT aggregation measurement by reduced and non-reduced blots under indicated doses of auranofin in 24-hour treatments. A red arrow marked the band of aggregated DLAT proteins. **e** measuring the lipoylation of DLAT protein under indicated doses of auranofin in 24-hour treatments. The DLAT protein in the treated cells was enriched by its cognate antibody before the detection of lipoylated DLAT by the anti-lipoylation antibody. For **c**–**e**, treatments were performed in RPMI + 10% FBS. **f** the molecular markers of cuproptosis under auranofin (5 μM) mono or combined treatments (TGTA, 20 μM; pantethine, 100 μM) in RPMI + 30% FBS. The samples derive from the same experiment, but different gels for anti-LIAS and anti-FDX1 antibodies were processed in parallel. For **b**, **d**–**f**, each blot is a representative of three biologically independent experiments. **g** cell viability assay comparing the boost effect of 2 μM elesclomol (ES) towards copper chloride (2 μM) and auranofin (2 μM) on HCT116 after a 24-hour incubation. Data are shown as mean ± s. d. of six independent experiments. Significance was calculated by unpaired, two-tailed *t*-test. **h** Effects of tetrathiomolybdate (50 μM) on cytotoxicity of copper chloride and auranofin treatments on HCT116 after a 24-hour incubation. The fold change of IC_{50} to that of the control group was shown. For **g**, **h**, treatments were performed in RPMI + 10% FBS, and data were presented as mean ± s. d. from 3 biologically independent replicates. Significance was calculated by an unpaired, two-tailed *t*-test. Significance was defined as $p < 0.05$. Source data are provided as a Source Data file.

in potentiating auranofin. Nonetheless, LA is endogenous and essential for metabolic regulation of the tricarboxylic acid (TCA) cycle via protein lipoylation[73]. It has been recently identified that internalized copper ions can target those lipoylated proteins and induce a type of cell death, coined cuproptosis[74]. Because of the high affinity of gold with thiols, it is possible for cellular gold(I) ions to dynamically interact with those disulfide-containing lipoylated proteins. Initially, we incubated auranofin with lipoic acid[75] in the cell lysates, observing hybrid gold-lipoic acid adducts by HRMS (Fig. 5a). Next, we investigated the molecular markers of the cuproptosis. FDX1 and LIAS are Fe-S cluster proteins involved in cuproptosis, showing a copper-dependent loss of protein levels. Then, we observed a decline of FDX1 and LIAS, either the mRNA or protein levels, in HCT116 cells upon auranofin treatment (Fig. 5b,c). The aggregate formation of DLAT protein, one of the lipoylated proteins, is another marker of cuproptosis[74]. As the blot showed, auranofin can induce the aggregation of DLAT (Fig. 5d) as well as a reduced level of lipoylated DLAT (Fig. 5e). In sum, the results suggested a cuproptosis-like mechanism induced by auranofin via gold-thiol exchanges.

Compared to auranofin mono-treatment, combos using either TGTA or pantethine further suppressed the protein level of LIAS and FDX1 in a dose-dependent manner (Fig. 5f and Supplementary Fig. 15a), in line with the ligand-enhanced cytotoxicity. Of interest, it has been reported that copper-induced cell death is regulated by its ionophore[74], or in other words, ligand[76]. Elesclomol (ES) dramatically promotes copper toxicity while tetrathiomolybdate (TTM) blocks[74]. By

comparing copper chloride and auranofin, we found ES prefers to enhance copper (Fig. 5g). In contrast, the thiolate-containing TTM can detoxify both copper and gold (Fig. 5h and Supplementary Fig. 15b), rendering a way to withdraw the gold cytotoxicity.

Discussion

The daunting range of drug resistance in tumors continuously demands new drugs with orthogonal targeting to the current ones[77]. A highly bioactive metal center coupled with easy-to-release ligands makes metallodrugs an efficient multitargeting agent, either used alone or as an adjuvant to other therapies[11]. However, the same ligand lability also results in a sophisticated behavior before and after they enter the tumor cells[15,78,79], exemplified by the rapid thiol exchange with albumin affecting the tumor uptake of auranofin. In this work, we put forward a strategy to recover serum-inhibited auranofin simply by adding nontoxic thiol ligands, indicating that albumin-auranofin interaction is in a modulable dynamic equilibrium. Despite the potential impact of thiol treatment on cellular processes that may contribute to the efficacy, the direct thiol-gold interaction mainly accounts for the elevated gold uptake in the presence of albumin-mediated blocking of gold ions. Subsequently, we confirmed that both the TGTA ligand of auranofin and other biocompatible small-molecule thiols can boost the antitumor activities of auranofin in multiple tumor models. Of note, the orally administered "auranofin + pantethine" combo produced an identical therapeutic outcome to cisplatin at 4 mg/kg in a mouse NSCLC model with a dosage of auranofin (0.9 mg/kg) equivalent to its approved use in rheumatoid arthritis. Since the primary target of auranofin is TrxR1, the intracellular activity of this protein, which specific fluorescent probes can detect, can be utilized as a biomarker for quickly determining effective thiol exchanges in future work. Also, the cuproptosis markers may be good alternatives. Together, our work illustrated that fast and dynamic ligand exchange can be utilized to realize an in vivo modulation of auranofin.

Two facets of our work may enlighten future studies in this field. Firstly, we illustrated how ligand-like small-molecule drugs can directly affect metallodrugs in a treatment regime. That is, the synergy between drugs may not only come from the target or pathway levels but also from a direct ligand exchange in a rapid way in vivo. Ligand-mediated effects on auranofin in our work are determined by the chemical features of ligands, e.g., hydrophobicity, consistent with previous reports[80,81]. Since thiol is one of the most common groups in bioactive molecules[82], a pool of ligands with diverse chemical properties can be envisioned to boost or halt the gold's toxicity to different degrees. That means an adjustable anticancer behavior even after the auranofin administration. Secondly, hydrophilic thiols that are preferred by some cell types may also potentiate auranofin in a much more selective manner. Encouraged by our discovery that auranofin plus CoA only works in the Jurkat T cell model, comparing the gene expression or dependency levels of Jurkat with other cell lines using well-established databases like DepMap[24,83] could potentially provide some hints for such a cell-specific activity of CoA. Subsequent studies to understand the cancer-enriched thiols may be fruitful as well. On the other hand, attaching thiol groups to already-in-use tumor-targeting agents such as small molecules, peptides[84,85], antibodies, and nanoparticles[86] seems a more feasible way for developing highly selective and effective anticancer combos with auranofin. Compared with developing novel drug candidates[11,12,15,38,61,87–102], screening relevant ligands directly with the initial gold complex obviates the need for a labor-intensive synthesis of structural derivatives.

Interestingly, the ligand issue has a relatively long history for metallodrugs, exemplified by the development of cisplatin. This pioneered metallodrug faced unacceptable nephrotoxicity in the early days of its development[103], which was attributed to the rapid hydrolysis of its chloride ligands to generate toxic platinum derivatives[104,105]. Later, such a problem was addressed using normal saline to dissolve the cisplatin in the clinical applications[106,107]. Using normal saline increased the concentration of chloride ions, equal to ligand supplementation. The excessive chloride ions inhibit the release of the chloride ligands of cisplatin, a dynamic ligand exchange manner, maintaining the drug in its original form[105–107]. This strategy may inspire the case of auranofin; at least we may consider a thiol-supplemented formula of auranofin to modulate its activities. Moreover, the ligand supplementation cases of cisplatin before and auranofin now indicate that our methods may be applied to other metallodrugs, as many of them possess labile ligands with relatively unpredictable manners in the serum. When selecting proper ligands, checking biological activities is still the priority. Then, in terms of ligand exchange, the chemical rules, such as the Hard-Soft-Acid-Base (HSAB) theory, can further aid the decision-making on which types of ligands should be tested first. For those already used metallodrugs, knowledge of the modulable nature highlighted in this work may be instructive to clinicians who are considering delicate adjustments of the activity and side toxicity using drug combos. Thus, we believe this work is of importance to the future development of metallodrugs either in mono or combined therapies.

Methods

Ethics statement

The research performed in the present study complies with all ethical regulations. The animal procedures were approved by the Research Ethics Committee of Sun Yat-Sen University (SYSU-IACUC-2020-0826) and conducted following the Guide for the Care and Use of Laboratory. All animals were purchased from the Experimental Animal Center of Sun Yat-Sen University (Guangzhou, China) and Nanjing Biomedical Research Institute of Nanjing University (Nanjing, China). All mice and rats were housed under specific-pathogen-free conditions and maintained in single-sex cages at 23 ± 3 °C and 40–70% humidity under a 12/12-h light/dark cycle. Inclusion criteria were: male or female, appropriate age and weight (15–30 g). Exclusion criteria were: tumor size must not exceed 15 mm (volume 2000 mm^3) in any direction in an adult mouse, tumor mass should not proceed to the point where it significantly interferes with normal bodily functions or causes pain or distress owing to its location, persistent self-induced trauma, rapid or progressive weight loss of more than 25%, for seven days. In none of the experiments were these approved ethical limits exceeded.

Cell lines and cell culture

Human cancer cell lines, including A549 (lung carcinoma cells), MDA-MB-231 (triple-negative breast cancer cells), HepG2 (hepatoma carcinoma cells), A375 (melanoma cells), PANC-1 (pancreatic carcinoma cells), and SW480 (colon adenocarcinoma cells), were from the American Type Culture Collection (ATCC). PC9 (lung carcinoma cells) were from the European Collection of Authenticated Cell Cultures (ECACC, London, UK). HCT116 (colon adenocarcinoma cells) were from the Procell company (Wuhan, China). Jurkat (human T lymphoblastic leukemia cells) were generously gifted by Guohui Wan at Sun Yat-Sen University. U87 (glioblastoma cells) were generously provided by the Min Feng group at Sun Yat-Sen University. PC9, A549, HCT116, and Jurkat were cultured using RPMI 1640 (Corning). HepG2, A375, PANC-1, SW480, MDA-MB-231, and U87 cells were cultured using DMEM (Thermo Fisher Scientific). All media were supplemented with 10% fetal bovine serum (Hyclone) and 1% penicillin-streptomycin G (Thermo Fisher Scientific).

Chemicals

Auranofin, 1-thio-β-D-glucose tetraacetate (TGTA), D-pantethine, R-pantetheine, cysteamine, calcium pantothenate, ammonium tetrathiomolybdate and bovine serum albumin (BSA) were purchased from Sigma-Aldrich. Disulfiram, β-D-glucose pentaacetate, coenzyme A, lipoic acid, dihydrolipoic acid, oltipraz, pyrithioxin dihydrochloride, and cisplatin were purchased from MedChemExpress. 1-thio-β-D-

Glucose (sodium salt) was purchased from Cayman. Elesclomol was purchased from TargetMol. Captopril was purchased from Selleck. Cremophor EL was purchased from Millipore. All chemicals were stored as stock solutions in DMSO or ultrapure water.

Mouse studies

All animal studies and procedures were conducted according to a protocol approved by the Research Ethics Committee of Sun Yat-Sen University. Mice were blindly randomized into different groups for treatment studies. Tumor volume was calculated with the equation V = (length × width^2)/2, and mouse body weight was also monitored during the study. For effects on PDX models, both the lung cancer PDX sample (ID: TM00192) and breast cancer PDX sample (ID: TM01273F707) are from the Jackson Laboratory, and we followed the previous protocol for PDX transplantation[108]. Lung cancer PDXs were transplanted by inserting 2 mm^3 into the dorsal flank of 4–6-week-old male NOD/SCID mice; breast cancer PDXs were transplanted by inserting 2 mm^3 into the dorsal flank of 4–6-week-old female NOD/SCID mice. When the volume of cancer PDX was approximately 40 mm^3, the mice were randomized and then treated intraperitoneally with 100 μL of either vehicle or 40 mg/kg TGTA (in corn oil) or 3 mg/kg AF (in a formulation of 15% Cremophor EL, 82.5% PBS and 2.5% DMSO) alone or combination treatment for 6 times per week.

For the establishment of HCT116 and A549 xenografts, 4–6-week-old male BALB/c nu/nu athymic mice with a body weight of 18–23 g were used. For evaluation of the effects of 'AF + TGTA' on human colon cell line xenografts, HCT116 cells were injected (2 × 10^6 cells transplanted subcutaneously) to grow tumors. When tumor volume had reached around 40 mm^3, mice were randomized into four treatment groups. The mice were then treated intraperitoneally with 100 μL of either vehicle or 40 mg/kg TGTA or 3 mg/kg AF alone or in combination treatment 6 times per week. One week was considered as one cycle.

For evaluation of the effects of 'AF + DPT' on human colon cell line xenografts, HCT116 cells were injected (2 × 10^6 cells transplanted subcutaneously) to grow tumors. When tumor volume had reached around 40 mm^3, mice were randomized into four treatment groups. The mice were then treated by oral gavage with 100 μL of either vehicle or 200 mg/kg D-pantethine (in saline) or 3 mg/kg AF alone or combination treatment. For evaluation of the effects of 'AF + DPT' on human lung cell line xenografts, A549 cells were injected (4 × 10^6 cells transplanted subcutaneously) to grow tumors. When tumor volume had reached around 40 mm^3, mice were randomized into three treatment groups. Mice were given 0.9 mg/kg AF and 200 mg/kg D-pantethine for combination treatment by oral gavage 2 times per week. The positive group was treated intraperitoneally with 100 μL of 4 mg/kg cisplatin (in saline) 2 times per week. One week was considered as one cycle.

Only female mice were used to study triple-negative breast cancer. All other animal models were conducted on male animals. Similar results were found in these experiments, seemingly no sex/gender issues were associated.

Gold uptake in the tumor site

4-6-week-old male BALB/c nu/nu athymic mice with a body weight of 18–23 g were used. HCT116 cells were injected (2 × 10^6 cells transplanted subcutaneously) to grow tumors. When tumor volumes had reached around 400 mm^3, mice were treated intraperitoneally with 3 mg/kg AF with and without 40 mg/kg TGTA for three consecutive days. Then, the mice were sacrificed with the tumor tissue isolated. The level of Au was examined by inductively coupled plasma mass spectrometry (ICP-MS) analysis.

Plasma gold studies in rats

Ten male Sprague-Dawley rats were equally divided into two groups. After fasting for 12 hours, the rats were given a single oral dose of auranofin (10 mg/kg) with or without pantethine (200 mg/kg). After 24 hours, the rats were treated orally with either saline or pantethine (200 mg/kg) again. The rats were placed in cages and 0.5 mL of heparinized blood was collected from each rat at 1.5, 6, 10, 24, 30, and 34 hours after administration of the drug. Approximately 0.5 mL of each blood specimen was transferred to a clean tube and centrifuged at 400 x *g* for 20 minutes. Plasma from each specimen was transferred to a clean tube with a dropping pipette. The collected plasma was digested with mixed acid (HNO_3:$HClO_4$ = 3:1) at 95 °C overnight. The same volume of ultrapure water was transferred into a separate EP tube for the background subtraction. Then, the concentration of Au in the plasma was examined with inductively coupled plasma mass spectrometry (ICP-MS) analysis.

Cell viability and growth assays

Cells were seeded in 96-well plates at 6000 cells per well and cultured for 24 hours before being subjected to various treatments. For the in-house ligand library screening, PC9 cells were used. Cells were treated with various ligands (50 μM) in the absence or presence of 5 μM AF in RPMI 1640 media supplemented with 30% fetal bovine serum. For the small-scale cell line profiling of pantethine, pantetheine, CoA, lipoic acid, and thioglucose, all cell lines were cultured in the human plasma-like medium (Gibco™) supplemented with 30% fetal bovine serum. After a total of 24 h treatment with indicated agents, cell viability was assessed using 20 μL of MTT (3-(4,5-dimethyl-2-thiazolyl)−2,5-diphenyl tetrazolium bromide) solutions and measured on a microplate spectrophotometer at a wavelength of 490 nm.

High-performance liquid chromatograms (HPLC)

High-performance liquid chromatograms were conducted with a reversed-phase C_{18} column at 214 nm to monitor the gold-thiol adducts[109]. The mobile phase consisted of a 65:35 solution of methanol-water with a flow rate of 1.0 ml/min. The column (length, 15 cm; inner diameter, 4.6 mm) was a Cosmosil model commercially packed with octadecylsilane reversed-phase material (code 38019-81). Experiments were performed at constant temperature (30 °C). Portions of 0.25 mol equivalent of a solution of auranofin (100 mM in 10 μL MeOH) were added to 1.0 mL of 4 mM solution of BSA and then reacted at 37 °C for 60 min in a shaker moving. The sample was divided into two aliquots of 250 μL each, one with 5.0 eq. TGTA (50 mM in MeOH) and one with an equal volume of methanol and the reaction was carried out for 20 minutes. Then all samples were precipitated by adding 4 times the amount of acetone (1.0 mL) and centrifuged at high speed for 10 minutes. The supernatant was filtered and then loaded into HPLC. All solutions were filtered through 0.22 μm membrane filters before use.

Determination of cellular TrxR activity

The cellular TrxR experiment was performed by using the Thioredoxin Reductase Activity Assay Kit (Solarbio)[110]. HCT116 cells were inoculated into a 6-well plate at the density of 2 × 10^5 cells per well and incubated for 36 h before being subjected to various treatments. After 1 h of incubation, the cells were washed three times with ice-cold PBS and then were added with 100 μL of ice-cold lysis buffer (50 mM phosphate buffer, pH 7.4, 1 mM EDTA, 0.1% Triton-X100). The protein concentrations were determined by BCA assay (Yeasen). Cellular TrxR activity was measured by a microplate Reader (OD 412 nm) according to the manufacturer's instructions.

ICP-MS experiments

For quantitative analysis of cellular uptake, U87 cells were seeded in 4 cm dishes at a density of 1 × 10^5 cells/ml (4.0 ml) and allowed to attach for 24 h. The cells were then treated with auranofin, disulfiram, and captopril (1:190:52) (3 μM) for 10 min at 37 °C in a CO_2 incubator. For cellular gold uptake of HCT116, cells were treated under 3 μM auranofin with or without thiol-containing drugs for 1 h. At the end of

the incubation, cells were collected and washed three times with ice-cold PBS. The collected cells were digested with mixed acid (HNO_3:$HClO_4$ = 3:1) at 95 °C overnight. The same volume of ultrapure water was transferred into a separate EP tube for the background subtraction, at least in duplicate per experiment. Then, the concentration of Au in the cells was examined with inductively coupled plasma mass spectrometry (ICP-MS, iCAP RQ) analysis. Values were normalized against protein content. All the samples were analyzed using three biological replicates.

Antibodies and western blotting

The following antibodies were used: polyclonal rabbit anti-LIAS (1:1,000; catalog no. 11577-1-AP; Proteintech); monoclonal rabbit anti-FDX1 (1:1,000; catalog no. ab108257; Abcam); monoclonal mouse anti-DLAT (1:1,000; catalog no. 12362S; Cell signaling Technology); monoclonal mouse HRP-conjugated GAPDH (1:10,000; catalog no. HRP-60004; Proteintech); polyclonal HRP-conjugated affinipure goat anti-mouse IgG(H + L) (1:10,000; catalog no. SA00001-1; Proteintech) and polyclonal HRP-conjugated affinipure goat anti-rabbit IgG(H + L) (1:10,000; catalog no. SA00001-2; Proteintech). HCT116 cells were inoculated into 4 cm tissue culture plates and grown to 75% confluence before being subjected to various treatments. The cells were washed three times with ice-cold PBS and then incubated with 100 μL of ice-cold lysis buffer supplemented with protease and phosphatase inhibitors (Sigma-Aldrich). Lysates were centrifuged at 10,000 x *g* at 4 °C for 12 min, and the protein concentration of the supernatant was determined using the BCA Protein Assay. 40 μg of protein per sample was mixed with sample buffer and denatured at 95 °C for 5 min. Samples were separated by SDS–PAGE and transferred to a nitrocellulose membrane. Membranes were blocked with 5% skim milk (Biofroxx) for 1 h at room temperature and then incubated with a 1:1,000 dilution of antibody at 4 °C overnight. Secondary antibodies were then incubated with the membrane for 1 h at room temperature, and the membrane was imaged using the Tanon Imaging System.

Chemical descriptor calculation

We manually constructed a molecular database file using CHEMDRAW and saved it in sdf format; subsequently, we opened this file in MOE, performed structure preparation via the Compute > Molecule > Wash function (selecting the "rebuild 3D" option under Coordinates), computed molecular descriptors using Compute > Descriptors > Calculate, and selected all descriptors excluding those categorized under "Protein" for calculation.

Evaluation of the chemical descriptors by randomForest

The descriptors' information of all the ligands (CSV file named "analysis2.csv") generated by MOE was used for evaluation. In this file, the first column is the ID number of each ligand with the heading "ID", and the second column is the cognate effectiveness information, headed as "class" with "Y" for the effective ones and "N" for the ineffective. The following columns were the chemical descriptors as calculated for each ligand. Then we started to use the R package "randomForest" (https://cran.r-project.org/package=randomForest) with the indicated code to evaluate these descriptors based on the factor of the "class" column in "analysis2.csv". The original data file "analysis2.csv" can be found in the Source data (Fig. 3d sheet), and the full code in R language has been shown in the Software and code section of the nr-reporting-summary file.

qRT-PCR

The HCT116 cells were treated with or without 4 μM auranofin for 12 hours before RNA extraction. The reverse transcription and qPCR were based on the UniPeak U+ One Step RT-qPCR SYBR Green Kit (catalog no. Q226; Vazyme), following the manufacturer's instructions. The primers for the genes of LIAS[111], GAPDH[112], and FDX[113] were listed below:

LIAS-forward, 5′-TGGTGTGACTACTTCAGAACCT-3′;
LIAS-reverse, 5′-GGAATAGGGCATGTGGATTTAGCA-3′;
GADPH-forward, 5′-AGGTCGGTGTGAACGGATTTG-3′
GADPH-reverse, 5′-TGTAGACCATGTAGTTGAGGTCA-3′
FDX-1-forward, 5′-TTCAACCTGTCACCTCATCTTTG-3′
FDX-1-reverse, 5′-TGCCAGATCGAGCATGTCATT-3′

High-resolution mass spectrometry (HRMS)

For the interaction between auranofin and the two clinical thiol drugs, the mixture of auranofin:disulfiram:captopril (1:1:2) (2 μM for auranofin) was prepared in analytical grade methanol before the HRMS detection. For evaluation of the modulation role of pantethine on auranofin in the human serum, auranofin (5 μM) and pantethine (25 μM) were incubated in the serum for 30 min at 37 °C. The sample was precipitated by adding methanol and centrifuged at high speed for 10 minutes. The supernatant was filtered through 0.22 μm filters and then loaded into HRMS (Waters SYNAPT G2-Si).

Statistics & Reproducibility

No statistical method was used to predetermine sample size. All results were presented as mean ± SD/SEM from at least three independent experiments. For in vivo experiments, we used at least 4 mice per group. For immunoblotting imaging, we performed at least 3 independent experiments. For biochemical and cell-based experiments, unless otherwise stated, $n = 3$ was chosen as the number of sample size. Significance was calculated by unpaired, two-tailed t-test.In animal experiments, mice and rats were randomly allocated into each experimental group. Data collection was performed by Molecular Operating Environment (MOE) software (version: 2015.10). Data analysis was conducted by the randonForest package of R language (version 4.3.1), Gaussian 16 and Microsoft Excel 2021. No data was excluded from this study. The Investigators were not blinded to allocation during experiments and outcome assessment.

Reporting summary

Further information on research design is available in the Nature Portfolio Reporting Summary linked to this article.

Data availability

The raw data of our transcriptomic profiling generated in this study have been deposited in the Genome Sequence Archive (GSA) with submission number subHRA016672 (title: HCT116-TGTA-50 uM-24 h, bioProject accession: PRJCA039268). The accession number to this data is HRA011270. The proteome raw data have been deposited to the ProteomeXchange Consortium via the PRIDE partner repository, with the dataset identifier PXD063241. The project name is "HCT116-TGTA-proteomic profiling". Source data are provided with this paper.

Code availability

The R language code of randomForest-based evaluation has been presented in the "Software and code" section of reporting summary. We uploaded the R language code to the Code Ocean with DOI as https://doi.org/10.24433/CO.3847399.v1 (URL: https://codeocean.com/capsule/3234223/tree/v1). Everyone can reproduce the evaluation outcome using our code and dataset in Code Ocean. Also, we included original dataset into the Source Data file.

References

1. Rottenberg, S., Disler, C. & Perego, P. The rediscovery of platinum-based cancer therapy. *Nat. Rev. Cancer* **21**, 37–50 (2021).
2. Forde, P. M. et al. Neoadjuvant Nivolumab plus Chemotherapy In Resectable Lung Cancer. *N. Engl. J. Med.* **386**, 1973–1985 (2022).

3. Wang, Z. X. et al. Toripalimab plus chemotherapy in treatment-naive, advanced esophageal squamous cell carcinoma (JUPITER-06): A multi-center phase 3 trial. *Cancer Cell* **40**, 277–288 (2022).
4. Liu, P. et al. PD-1 blockade synergizes with oxaliplatin-based, but not cisplatin-based, chemotherapy of gastric cancer. *Oncoimmunology* **11**, 2093518 (2022).
5. Pfirschke, C. et al. Immunogenic chemotherapy sensitizes tumors to checkpoint blockade therapy. *Immunity* **44**, 343–354 (2016).
6. Petroni, G., Kroemer, G. & Galluzzi, L. Immunogenic therapies drive CAR T cells towards superior efficacy. *Trends Cancer* **7**, 179–181 (2021).
7. Bertini, I. G., Harry B., Lippard, S. J., Valentine, J. S. *Bioinorganic Chemistry* (University Science Books, 1994).
8. Nagai, N., Okuda, R., Kinoshita, M. & Ogata, H. Decomposition kinetics of cisplatin in human biological fluids. *J. Pharm. Pharmacol.* **48**, 918–924 (1996).
9. Wang, D. & Lippard, S. J. Cellular processing of platinum anticancer drugs. *Nat. Rev. Drug Discov.* **4**, 307–320 (2005).
10. Cini, M., Bradshaw, T. D. & Woodward, S. Using titanium complexes to defeat cancer: the view from the shoulders of titans. *Chem. Soc. Rev.* **46**, 1040–1051 (2017).
11. Anthony, E. J. et al. Metallodrugs are unique: opportunities and challenges of discovery and development. *Chem. Sci.* **11**, 12888–12917 (2020).
12. Casini, A. & Pothig, A. Metals in cancer research: beyond platinum metallodrugs. *ACS Cent. Sci.* **10**, 242–250 (2024).
13. Mertens, R. T., Gukathasan, S., Arojojoye, A. S., Olelewe, C. & Awuah, S. G. Next generation gold drugs and probes: chemistry and biomedical applications. *Chem. Rev.* **123**, 6612–6667 (2023).
14. Zou, T., Lum, C. T., Lok, C.-N., Zhang, J.-J. & Che, C.-M. Chemical biology of anticancer gold(III) and gold(I) complexes. *Chem. Soc. Rev.* **44**, 8786–8801 (2015).
15. Riccardi, L., Genna, V. & De Vivo, M. Metal-ligand interactions in drug design. *Nat. Rev. Chem.* **2**, 100–112 (2018).
16. Zou, T. et al. Anticancer metal-N-heterocyclic carbene complexes of gold, platinum and palladium. *Curr. Opin. Chem. Biol.* **43**, 30–36 (2018).
17. Jiang, J., Xiong, X. & Zou, T. Modulating the chemical reactivity of gold complexes in living systems: from concept to biomedical applications. *Acc. Chem. Res.* **56**, 1043–1056 (2023).
18. Tong, K. C. et al. An anticancer gold(III)-activated porphyrin scaffold that covalently modifies protein cysteine thiols. *Proc. Natl. Acad. Sci. USA.* **117**, 1321–1329 (2020).
19. Johnson, A. et al. The anti-breast cancer stem cell properties of gold(I)-non-steroidal anti-inflammatory drug complexes. *Chem. Sci.* **14**, 557–565 (2023).
20. Arojojoye, A. S. et al. Serum-Stable Gold(III) Bisphosphine complex induces mild mitochondrial uncoupling and in vivo antitumor potency in triple negative breast cancer. *J. Med. Chem.* **66**, 7868–7879 (2023).
21. Kim, J. H. et al. Anticancer gold(III)-bisphosphine complex alters the mitochondrial electron transport chain to induce in vivo tumor inhibition. *Chem. Sci.* **12**, 7467–7479 (2021).
22. Corsello, S. M. et al. The Drug Repurposing Hub: a next-generation drug library and information resource. *Nat. Med.* **23**, 405–408 (2017).
23. Beijersbergen, R. L. Old drugs with new tricks. *Nat. Cancer* **1**, 153–155 (2020).
24. Corsello, S. M. et al. Discovering the anti-cancer potential of non-oncology drugs by systematic viability profiling. *Nat. Cancer* **1**, 235–248 (2020).
25. Gyawali, B., Bouche, G., Crisp, N. & Andre, N. Challenges and opportunities for cancer clinical trials in low- and middle-income countries. *Nat. Cancer* **1**, 142–145 (2020).
26. Yuan, S. F. et al. Metallodrug ranitidine bismuth citrate suppresses SARS-CoV-2 replication and relieves virus-associated pneumonia in Syrian hamsters. *Nat. Microbiol.* **5**, 1439–1448 (2020).
27. Harris, I. S. et al. Glutathione and Thioredoxin antioxidant pathways synergize to drive cancer initiation and progression. *Cancer Cell* **27**, 211–222 (2015).
28. Ali, S. A., Justilien, V., Jamieson, L., Murray, N. R. & Fields, A. P. Protein Kinase Cι drives a NOTCH3-dependent Stem-like Phenotype in Mutant KRAS Lung Adenocarcinoma. *Cancer Cell* **29**, 367–378 (2016).
29. Hayes, J. D., Dinkova-Kostova, A. T. & Tew, K. D. Oxidative stress in cancer. *Cancer Cell* **38**, 167–197 (2020).
30. Nobili, S. et al. Gold compounds as anticancer agents: chemistry, cellular pharmacology, and preclinical studies. *Med. Res. Rev.* **30**, 550–580 (2010).
31. Hatem, E. et al. Auranofin/Vitamin C: A novel drug combination targeting triple-negative breast cancer. *J. Natl. Cancer Inst.* **111**, 597–608 (2019).
32. Lee, D. et al. Induction of oxidative stress through inhibition of Thioredoxin Reductase 1 Is an effective therapeutic approach for hepatocellular carcinoma. *Hepatology* **69**, 1768–1786 (2019).
33. Shen, S. Y., Shen, J., Luo, Z., Wang, F. D. & Min, J. X. Molecular mechanisms and clinical implications of the gold drug auranofin. *Coord. Chem. Rev.* **493**, 215323 (2023).
34. Gamberi, T. et al. Upgrade of an old drug: Auranofin in innovative cancer therapies to overcome drug resistance and to increase drug effectiveness. *Med. Res. Rev.* **42**, 1111–1146 (2022).
35. Berners-Price, S. J. et al. In vivo antitumor activity and in vitro cytotoxic properties of bis[1,2-bis(diphenylphosphino)ethane] gold(I) chloride. *Cancer Res.* **46**, 5486–5493 (1986).
36. Sadler, P. J. & Sue, R. E. The chemistry of gold drugs. *Met. -Based Drugs* **1**, 107–144 (1994).
37. Shaw, C. F. Gold-based therapeutic agents. *Chem. Rev.* **99**, 2589–2600 (1999).
38. Milacic, V. et al. A novel anticancer gold(III) dithiocarbamate compound inhibits the activity of a purified 20S proteasome and 26S proteasome in human breast cancer cell cultures and xenografts. *Cancer Res.* **66**, 10478–10486 (2006).
39. Hickey, J. L. et al. Mitochondria-targeted chemotherapeutics: The rational design of gold(I) N-heterocyclic carbene complexes that are selectively toxic to cancer cells and target protein selenols in preference to thiols. *J. Am. Chem. Soc.* **130**, 12570–12571 (2008).
40. Ott, I. On the medicinal chemistry of gold complexes as anticancer drugs. *Coord. Chem. Rev.* **253**, 1670–1681 (2009).
41. Ralph, S. J., Nozuhur, S., RA, A. L., Rodriguez-Enriquez, S. & Moreno-Sanchez, R. Repurposing drugs as pro-oxidant redox modifiers to eliminate cancer stem cells and improve the treatment of advanced stage cancers. *Med. Res. Rev.* **39**, 2397–2426 (2019).
42. Zhang, J.-J. et al. A multitarget Gold(I) complex induces cytotoxicity related to Aneuploidy in HCT-116 colorectal carcinoma cells. *Angew. Chem. Int. Ed.* **59**, 16795–16800 (2020).
43. Cosottini, L. et al. Bioconjugation of the gold drug auranofin to human ferritin yields a potent cytotoxin. *J. Drug. Deliv. Sci. Tec.* **87**, 104822–104831 (2023).
44. Moreno-Alcantar, G., Picchetti, P. & Casini, A. Gold complexes in anticancer therapy: from new design principles to particle-based delivery systems. *Angew. Chem. Int. Ed.* **62**, e202218000 (2023).
45. Zhang, J. B. et al. Systematic identification of anticancer drug targets reveals a nucleus-to-mitochondria pathway. *Cell* **186**, 2361–2379 (2023).
46. Landini, I. et al. Selection and characterization of a human ovarian cancer cell line resistant to auranofin. *Oncotarget* **8**, 96062–96078 (2017).

47. Gamberi, T., Pratesi, A., Messori, L. & Massai, L. Proteomics as a tool to disclose the cellular and molecular mechanisms of selected anticancer gold compounds. *Coord. Chem. Rev.* **438**, 213905 (2021).
48. Chiappetta, G. et al. Redox proteome analysis of auranofin exposed ovarian cancer cells (A2780). *Redox Biol.* **52**, 102294 (2022).
49. Snyder, R. M., Mirabelli, C. K. & Crooke, S. T. Cellular association, intracellular distribution, and efflux of auranofin via sequential ligand exchange reactions. *Biochem. Pharmacol.* **35**, 923–932 (1986).
50. Coffer, M. T., Shaw, C. F., Hormann, A. L., Mirabelli, C. K. & Crooke, S. T. Thiol competition for Et_3PAuS-albumin: a nonenzymatic mechanism for Et_3PO formation. *J. Inorg. Biochem.* **30**, 177–187 (1987).
51. Roberts, J. R., Xiao, J., Schliesman, B., Parsons, D. J. & Shaw, C. F. Kinetics and mechanism of the reaction between serum albumin and auranofin (and its isopropyl analogue) in vitro. *Inorg. Chem.* **35**, 424–433 (1996).
52. Simon, T. M., Kunishima, D. H., Vibert, G. J. & Lorber, A. Screening trial with the coordinated gold compound auranofin using mouse lymphocyte leukemia P388. *Cancer Res.* **41**, 94–97 (1981).
53. Mirabelli, C. K. et al. Evaluation of the in vivo antitumor activity and in vitro cytotoxic properties of auranofin, a coordinated gold compound, in murine tumor models. *Cancer Res.* **45**, 32–39 (1985).
54. Saba, N. S. et al. Auranofin induces a reversible in-vivo stress response that correlates with a transient clinical effect in patients with chronic lymphocytic leukemia. *Blood* **122**, 3819–3819 (2013).
55. Halatsch, M. E. et al. Bcl-2/Bcl-xL inhibition predominantly synergistically enhances the anti-neoplastic activity of a low-dose CUSP9 repurposed drug regime against glioblastoma. *Br. J. Pharmacol.* **176**, 3681–3694 (2019).
56. Halatsch, M. E. et al. A phase Ib/IIa trial of 9 repurposed drugs combined with temozolomide for the treatment of recurrent glioblastoma: CUSP9v3. *Neurooncol. Adv.* **3**, vdab075 (2021).
57. Skrott, Z. et al. Alcohol-abuse drug disulfiram targets cancer via p97 segregase adaptor NPL4. *Nature* **552**, 194–199 (2017).
58. Bindoli, A. et al. Thioredoxin reductase: A target for gold compounds acting as potential anticancer drugs. *Coord. Chem. Rev.* **253**, 1692–1707 (2009).
59. Casini, A., Wai-Yin Sun, R. & Ott, I. *Metallo-Drugs: Development and Action of Anticancer Agents* (De Gruyter, 2018).
60. Pickering, I. J. et al. Direct observation of Methylmercury and Auranofin binding to Selenocysteine in Thioredoxin Reductase. *Inorg. Chem.* **59**, 2711–2718 (2020).
61. Busker, S., Page, B. & Arnér, E. S. J. To inhibit TrxR1 is to inactivate STAT3–Inhibition of TrxR1 enzymatic function by STAT3 small molecule inhibitors. *Redox Biol.* **36**, 101646 (2020).
62. Yan, X. et al. Inhibition of Thioredoxin/Thioredoxin Reductase induces synthetic lethality in lung cancers with compromised Glutathione Homeostasis. *Cancer Res* **79**, 125–132 (2019).
63. Raninga, P. V. et al. Therapeutic cooperation between auranofin, a thioredoxin reductase inhibitor and anti-PD-L1 antibody for treatment of triple-negative breast cancer. *Int. J. Cancer* **146**, 123–136 (2020).
64. Yin, N. et al. Protein kinase Cı mediates immunosuppression in lung adenocarcinoma. *Sci. Transl. Med.* **14**, eabq5931 (2022).
65. Chen, S. Y. et al. Diphenyl disulfide potentiates the apoptosis of breast cancer cells through Bax proteolytic activation with accompanying autophagy. *Environ. Toxicol.* **38**, 2022–2030 (2023).
66. Sibon, O. C. M. & Strauss, E. Coenzyme A: to make it or uptake it?. *Nat. Rev. Mol. Cell Biol.* **17**, 605–606 (2016).
67. McRae, M. P. Treatment of hyperlipoproteinemia with pantethine: A review and analysis of efficacy and tolerability. *Nutr. Res.* **25**, 319–333 (2005).
68. Srinivasan, B. et al. Extracellular 4′-phosphopantetheine is a source for intracellular coenzyme A synthesis. *Nat. Chem. Biol.* **11**, 784–792 (2015).
69. Gottlieb, N. L. Pharmacology of auranofin: overview and update. *Scand. J. Rheumatol. Suppl.* **63**, 19–28 (1986).
70. Debnath, A. et al. A high-throughput drug screen for Entamoeba histolytica identifies a new lead and target. *Nat. Med.* **18**, 956–960 (2012).
71. Blocka, K. Auranofin versus injectable gold: Comparison of pharmacokinetic properties. *Am. J. Med.* **75**, 114–122 (1983).
72. Walz, D. T., DiMartino, M. J., Griswold, D. E., Intoccia, A. P. & Flanagan, T. L. Biologic actions and pharmacokinetic studies of auranofin. *Am. J. Med.* **75**, 90–108 (1983).
73. Solmonson, A. & DeBerardinis, R. J. Lipoic acid metabolism and mitochondrial redox regulation. *J. Biol. Chem.* **293**, 7522–7530 (2018).
74. Tsvetkov, P. et al. Copper induces cell death by targeting lipoylated TCA cycle proteins. *Science* **375**, 1254–1261 (2022).
75. Smith, A. R., Shenvi, S. V., Widlansky, M., Suh, J. H. & Hagen, T. M. Lipoic acid as a potential therapy for chronic diseases associated with oxidative stress. *Curr. Med. Chem.* **11**, 1135–1146 (2004).
76. Steinbrueck, A. et al. Transition metal chelators, pro-chelators, and ionophores as small molecule cancer chemotherapeutic agents. *Chem. Soc. Rev.* **49**, 3726–3747 (2020).
77. Holohan, C., Van Schaeybroeck, S., Longley, D. B. & Johnston, P. G. Cancer drug resistance: an evolving paradigm. *Nat. Rev. Cancer* **13**, 714–726 (2013).
78. Hong, Y., Lai, Y., Chan, G. & Sun, H. Glutathione and multidrug resistance protein transporter mediate a self-propelled disposal of bismuth in human cells. *Proc. Natl. Acad. Sci. USA* **112**, 3211–3216 (2015).
79. Romero-Canelón, I. & Sadler, P. J. Systems approach to metal-based pharmacology. *Proc. Natl. Acad. Sci. USA* **112**, 4187–4188 (2015).
80. Marzo, T. et al. Auranofin, Et3PAuCl, and Et3PAuI ARE HIGHLY CYTOTOXIC ON COLORECTAL CANCER CELLS: A CHEMICAL AND BIOLOGICAL Study. *ACS Med. Chem. Lett.* **8**, 997–1001 (2017).
81. Marzo, T. et al. Replacement of the Thiosugar of Auranofin with Iodide enhances the anticancer potency in a mouse model of ovarian cancer. *ACS Med. Chem. Lett.* **10**, 656–660 (2019).
82. Ertl, P., Altmann, E. & McKenna, J. M. The most common functional groups in bioactive molecules and how their popularity has evolved over time. *J. Med. Chem.* **63**, 8408–8418 (2020).
83. Meyers, R. M. et al. Computational correction of copy number effect improves specificity of CRISPR-Cas9 essentiality screens in cancer cells. *Nat. Genet.* **49**, 1779–1784 (2017).
84. Marciano, Y. et al. Encapsulation of gold-based anticancer agents in Protease-degradable peptide nanofilaments enhances their potency. *J. Am. Chem. Soc.* **145**, 234–246 (2023).
85. Batchelor, L. K., De Falco, L., Dyson, P. J. & Davey, C. A. Viral peptide conjugates for metal-warhead delivery to chromatin. *RSC Adv.* **14**, 8718–8725 (2024).
86. Cosottini, L. et al. Unlocking the power of human ferritin: enhanced drug delivery of Aurothiomalate in A2780 ovarian cancer cells. *Angew. Chem. Int. Ed.* **63**, e202410791 (2024).
87. Messori, L. et al. Gold(III) complexes as potential antitumor agents: Solution chemistry and cytotoxic properties of some selected gold(III) compounds. *J. Med. Chem.* **43**, 3541–3548 (2000).
88. Lu, Y. L. et al. Recent development of gold(I) and gold(III)complexes as therapeutic agents for cancer diseases. *Chem. Soc. Rev.* **51**, 5518–5556 (2022).
89. Wragg, D. et al. On the mechanism of Gold/NHC compounds binding to DNA G-Quadruplexes: combined metadynamics and biophysical methods. *Angew. Chem. Int. Ed.* **57**, 14524–14528 (2018).

90. Sulaiman, A. A. A. et al. Design, synthesis, and preclinical activity in ovarian cancer models of new Phosphanegold(I)-N-heterocyclic Carbene complexes. *J. Med. Chem.* **65**, 14424–14440 (2022).
91. Babu, T. et al. Oral anticancer heterobimetallic PtIV–AuI complexes show high in vivo activity and low toxicity. *Angew. Chem. Int. Ed.* **62**, e202217233 (2023).
92. Meyer, A. et al. On the biological properties of alkynyl phosphine Gold(I) complexes. *Angew. Chem. Int. Ed.* **51**, 8895–8899 (2012).
93. Fernández-Gallardo, J. et al. Heterometallic titanium–gold complexes inhibit renal cancer cells in vitro and in vivo. *Chem. Sci.* **6**, 5269–5283 (2015).
94. Zhou, X.-Q. et al. In vivo metallophilic self-assembly of a light-activated anticancer drug. *Nat. Chem.* **15**, 980–987 (2023).
95. Zhou, X.-Q. et al. Multitarget Thiol-Activated Tetrapyridyl Gold(III) complexes for hypoxic cancer therapy. *CCS Chem.* **6**, 783–797 (2023).
96. Zhou, X.-Q. et al. Rollover Cyclometalation vs nitrogen coordination in Tetrapyridyl Anticancer Gold(III) complexes: effect on protein interaction and toxicity. *JACS Au* **1**, 380–395 (2021).
97. López-Hernández, J. E. & Contel, M. Promising heterometallic compounds as anticancer agents: Recent studies in vivo. *Curr. Opin. Chem. Biol.* **72**, 102250 (2023).
98. Batchelor, L. K. et al. Crosslinking allosteric sites on the nucleosome. *Angew. Chem. Int. Ed.* **58**, 15660–15664 (2019).
99. Adhireksan, Z. et al. Allosteric cross-talk in chromatin can mediate drug-drug synergy. *Nat. Commun.* **8**, 14860 (2017).
100. Cheff, D. M. et al. The ferroptosis inducing compounds RSL3 and ML162 are not direct inhibitors of GPX4 but of TXNRD1. *Redox Biol.* **62**, 102703 (2023).
101. Busschaert, N. et al. A synthetic ion transporter that disrupts autophagy and induces apoptosis by perturbing cellular chloride concentrations. *Nat. Chem.* **9**, 667–675 (2017).
102. Sen, S. et al. Rationally designed Redox-Active Au(I) N-heterocyclic carbene: an immunogenic cell death inducer. *J. Am. Chem. Soc.* **142**, 20536–20541 (2020).
103. Loehrer, P. J. & Einhorn, L. H. Cisplatin. *Ann. Intern. Med.* **100**, 704–713 (1984).
104. Blachley, J. D. & Hill, J. B. Renal and electrolyte disturbances associated with Cisplatin. *Ann. Intern. Med.* **95**, 628–632 (1981).
105. Daley-Yates, P. T. & McBrien, D. C. H. A study of the protective effect of chloride salts on cisplatin nephrotoxicity. *Biochem. Pharmacol.* **34**, 2363–2369 (1985).
106. Crona, D. J. et al. A systematic review of strategies to prevent Cisplatin-Induced Nephrotoxicity. *Oncologist* **22**, 609–619 (2017).
107. Sainamthip, P., Saichaemchan, S., Satirapoj, B. & Prasongsook, N. The effect of intravenous mannitol combined with normal saline in preventing cisplatin-induced nephrotoxicity: a randomized, double-blind, placebo-controlled trial. *JCO Glob. Oncol.* **8**, e2100275 (2022).
108. Cai, D. M. et al. ROR gamma is a targetable master regulator of cholesterol biosynthesis in a cancer subtype. *Nat. Commun.* **10**, 4621 (2019).
109. Tepperman, K. et al. Intestinal uptake and metabolism of auranofin, a new oral gold-based antiarthritis drug. *Science* **225**, 430–432 (1984).
110. Luo, Y. et al. Organogold(III) complexes display conditional photoactivities: evolving from photodynamic into photoactivated chemotherapy in response to o-2 consumption for robust cancer therapy. *Angew. Chem. Int. Ed.* **61**, e202212689 (2022).
111. Jiang, M. et al. Verification of cuproptosis-related diagnostic model associated with immune infiltration in rheumatoid arthritis. *Front. Endocrinol.* **14**, 1204926 (2023).
112. Liu, K. et al. Impaired macrophage autophagy increases the immune response in obese mice by promoting proinflammatory macrophage polarization. *Autophagy* **11**, 271–284 (2015).
113. Wang, W. et al. Ferroptosis inducers enhanced cuproptosis induced by copper ionophores in primary liver cancer. *J. Exp. Clin. Cancer Res.* **42**, 142 (2023).

Acknowledgements

This work was finically supported by the National Natural Science Foundation of China (nos. 22377154, 22122706 and 32100058), Major Program of Guangzhou National Laboratory (GZNL2023A02012), Guangdong Science and Technology Department (no. 2019QN01C125), Guangdong Basic and Applied Basic Research Foundation (no. 2024A1515010721 and 2024B1515040028), Guangzhou Science and Technology Projects (no. 2024A04J6478), and Guangdong Provincial Key Laboratory of Construction Foundation (no. 2023B1212060022).

Author contributions

T.Z. conceived and designed the study. Y.W., B.C., Q.W., S.Z., X.F., J.W., A.S.C.C., X.X., and T.Z. designed and performed the experiments. X.X., Y.W., and T.Z. contributed to the writing and editing of the manuscript and all authors approved the final edition of the manuscript. Supervision was provided by J.W., X.X., and T.Z.

Competing interests

Y.W., X.X., A.S.C.C., and T.Z. hold patents related to combo treatment by auranofin and thiols/disulfides. The remaining authors declare no competing interests.

Additional information

Supplementary information The online version contains supplementary material available at https://doi.org/10.1038/s41467-025-62634-9.

Correspondence and requests for materials should be addressed to Junjian Wang, Xiaolin Xiong or Taotao Zou.

Peer review information *Nature Communications* thanks Tiziano Marzo, and the other, anonymous, reviewer(s) for their contribution to the peer review of this work. A peer review file is available.